Dynamic Improvement of Series-Series Compensated Wireless Power Transfer Systems Using Discrete Sliding Mode Control

Yun Yang, *Student Member, IEEE*, Wenxing Zhong, *Member, IEEE*, Sitthisak Kiratipongvoot, Siew-Chong Tan, *Senior Member, IEEE* and S. Y. Ron Hui, *Fellow, IEEE*

***Abstract*--This paper presents a discrete sliding mode control (DSMC) scheme for a series-series compensated wireless power transfer (WPT) system to achieve fast maximum energy efficiency (MEE) tracking and output voltage regulation. The power transmitter of the adopted WPT system comprises a DC/AC converter, which incorporates the hill-climbing-search-based phase angle control in achieving minimum input current injection from its DC source, thereby attaining minimum input power operation. The power receiver comprises a buck-boost converter that emulates an optimal load value, following the MEE point determined by the DSMC scheme. With this WPT system, no direct communication means is required between the transmitter and the receiver. Therefore, the implementation cost of this system is potentially lower and annoying communication delays which deteriorate control performance are absent. Both the simulation and experiment results show that this WPT system displays better dynamic regulation of the output voltage during MEE tracking when it is controlled by DSMC, as compared to that controlled by the conventional discrete proportional-integral (PI) control. Such an improvement prevents the load from sustaining undesirable overshoot/undershoot during transient states.**

***Index Terms*--Discrete sliding mode control (DSMC), series-series compensated wireless power transfer (WPT) system, maximum energy efficiency (MEE), hill-climbing-search-based phase angle control, dynamic performance.**

I. Introduction

EVER since the patent of wireless power transfer (WPT) based on magnetic resonance and near-field coupling of two-loop resonators was reported by Nikola Tesla in 1914 [1], the WPT technique has been widely applied in medical implants [2]−[4], induction heaters [5], electric vehicles [6]−[8] and wireless charging platforms for portable equipment such as cellphones [9]−[14]. Particularly over the last decade, with the emergence of diverse mobile terminals, the "Qi" standard is established by the Wireless Power Consortium (covering over 210 companies worldwide in over 16 countries) [15] for more than 600 products [16]. Meanwhile, research activities of WPT systems have intensified in aspects relating to magnetic coupling [17]−[21], circuit compensation [7], [8], [21], [22], modeling and control [23]−[28], and basic operating principles, such as maximum power transfer (MPT) principle and maximum energy efficiency (MEE) principle [21], [28], [29]. In the review given in [29], it has been clarified that the MPT principle and the MEE principle should be respectively used for specific applications. WPT systems operating under the MPT principle will never achieve a system's energy efficiency of higher than 50%. However, its achievable transmission distance is longer than that of the same WPT systems operating under the MEE principle. Nevertheless, WPT systems operating under the MEE principle can easily achieve an energy efficiency of higher than 50%.

In this paper, the MEE principle is adopted for the investigated WPT system with series-series compensation. The decision on using this compensation instead of series-parallel compensation, parallel-parallel compensation, or parallel-series compensation is because the series-series compensation is independent of load or mutual inductance [25]. However, series-series compensated WPT systems that operate under the MEE principle suffers from power-efficiency variation when the coupling coefficient, quality factor, and load conditions change [26]−[28]. A mismatch of these parameters between the designed system and the actual system will result in a reduction of system's energy efficiency. To resolve this issue, dynamic MEE tracking schemes are adopted in WPT systems operating in MEE, as reported in [26]−[28]. In [28], the automatic MEE tracking scheme involves a switched-mode converter at the receiver side to emulate the optimal load of minimizing the input power at the transmitter. This scheme is free of communication between the transmitter and the receiver. While it performs accurate tracking of MEE and output voltage regulation at steady state, it does not give good dynamic regulation of the output voltage during the MEE tracking process. Here, the series-series compensated WPT system is controlled by a discrete PI control scheme. It performs poorly in responding to fast dynamic changes of coupling coefficient, quality factor, and load conditions, of which the process of MEE tracking may induce large overshoot/undershoot and longer settling time of the output voltage. This may shorten the lifetime and even damage the load in which it is connected to.

Manuscript received June 9, 2017; revised July 27, 2017; accepted August 26, 2017. This work is supported by the Hong Kong Research Grant Council under Theme-based Research Project: T23-701/14-N.

Y. Yang, S. Kiratipongvoot, and S. C. Tan are with the Department of Electrical and Electronic Engineering, The University of Hong Kong, Hong Kong, China (e-mail: cacalotoyangyun@gmail.com, ksitthis@eee.hku.hk, sctan@eee.hku.hk).

W. Zhong is with the Department of Electrical Engineering, Zhejiang University, Hangzhou, China (e-mail: wxzhong@zju.edu.cn).

S. Y. R. Hui is with the Department of Electrical and Electronic Engineering, The University of Hong Kong, Hong Kong, China and also with the Department of Electrical and Electronic Engineering, Imperial College London, London SW7 2AZ, U.K. (e-mail: ronhui@eee.hku.hk).

To achieve a consistent and optimized dynamic performance of the series-series compensated WPT system in the event of unknown and wide-range changes, it is proposed in this paper, to replace the discrete PI control scheme with a discrete sliding mode control (DSMC) scheme. Sliding mode control (SMC) is naturally well suited for the control of power converters [30]. It consists of a time-varying state-feedback discontinuous control law that switches at a high frequency from one continuous structure to another according to the present position of the state variables in the state space. SMC offers superior dynamic performance for power converters in a wide operating range [31]. However, most of the SMC are implemented in analog controller forms [32]−[34]. Studies on DSMC for digital controllers are relatively limited [35]−[37], much less the applications [38], [39]. The applied DSMC for the WPT system is inherited from the equivalent SMC described in [32]. The implementation of the DSMC can be briefly described as a derived equivalent control signal based on the discrete SMC law to be modulated by the time-based counter of digital controllers. Compared to conventional discrete PI control, only one more current sensor for the output capacitor current is required.

In the proposed work, a hill-climbing-search-based phase angle control is used with the DC/AC converter to achieve minimum input current, thereby attaining minimum input power control. The algorithm of the phase angle control is designed by considering the working principle of digital controllers. The phase angle control renders the series-series compensated WPT system with MEE, but does not contribute to the dynamic improvement. Still, the dynamic improvement of the output voltage is still significant when the series-series compensated WPT system is controlled by the proposed DMSC scheme. This paper is an extension of the conference paper [40].

II. Difference Between MEE and MPT of the WPT System

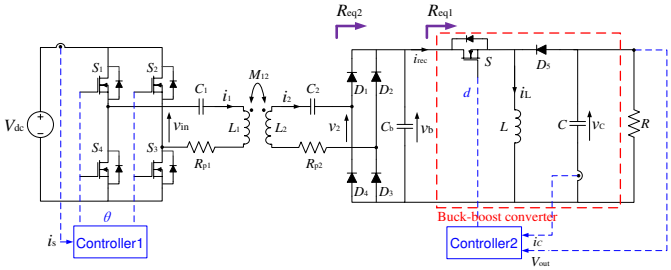

Fig. 1. Schematic diagram of the series-series compensated WPT system with non-communication controllers.

A schematic diagram of the series-series compensated WPT system is depicted as shown in Fig. 1, where V_{dc} is the DC power supply; L_1 and L_2 are the self-inductance of the primary and the secondary windings; R_{p1} and R_{p2} are the equivalent resistances of the primary and the secondary windings, respectively; M_{12} is the mutual inductance of the two windings; C_1 and C_2 denotes the compensating capacitors required for compensating the large leakage inductance and also for blocking the DC voltage offset caused by the inverting bridge; C_b is the filtering capacitance; L and C are the energy storage components of the buck-boost converter; and R is the resistance of load.

In Fig. 1, the buck-boost converter (on the right-side of the figure) can operate in continuous conduction mode (CCM) or discontinuous conduction mode (DCM), depending upon the inductance value of L. If $L \geq \frac{D(1-D)V_{dc}}{2i_L f_{s1}}$, where D is the duty ratio of switch S, i_L is the inductor current, and f_{s1} is the switching frequency, the buck-boost converter is operating in CCM with a load R, which has a corresponding equivalent impedance of

$$R_{eq1CCM} = \frac{(1-D)^2}{D^2} R. \tag{1}$$

Conversely, if $L < \frac{D(1-D)V_{dc}}{2i_L f_{s1}}$, the buck-boost converter operates in DCM with the load R with an equivalent impedance of

$$R_{eq1DCM} = \frac{2Lf_{s1}}{D^2}. \tag{2}$$

By taking both (1) and (2) into consideration, the equivalent impedance can be generally expressed as

$$R_{eq1} = \frac{\left[(1-D)^2 R - 2Lf_{s1}\right]\kappa + 2Lf_{s1}}{D^2}, \tag{3}$$

where $\kappa \epsilon \{0,1\}$. κ=1 indicates that the buck-boost converter is operating in CCM and κ=0 indicates that it is operating in DCM.

An equivalent impedance R_{eq2} can be further derived from equation (3) by incorporating the diode rectifier and the filtering capacitor C_b. Based on the extended describing function [24], all the higher harmonics can be neglected as the resonant tank is tuned to fundamental harmonic as $v_2 = \frac{4}{\pi} v_b(\omega t)$, where ω=2πf_s, f_s is the switching frequency of the DC/AC converter. Then, the root-mean-square (RMS) value of v_2 is $\frac{2\sqrt{2}}{\pi} v_b$. Similarly, the RMS value of i_2 can be derived as $\frac{\sqrt{2}\pi}{4} i_{rec}$. Hence, the equivalent impedance R_{eq2} is

$$R_{eq2} = \frac{v_{2rms}}{i_{2rms}} = \frac{8}{\pi^2} R_{eq1} = \frac{\left[8(1-D)^2 R - 16Lf_{s1}\right]\kappa + 16Lf_{s1}}{\pi^2 D^2}, \tag{4}$$

where v_{2rms} is the RMS value of v_2 and i_{2rms} is the RMS value of i_2.

A simplified schematic diagram of the series-series compensated WPT system expressed in terms of the equivalent impedance can be drawn as shown in Fig. 2.

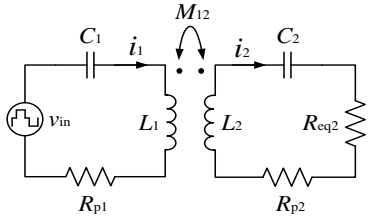

Fig. 2. Simplified schematic diagram of the series-series compensated WPT system.

Then, the energy efficiency of the system can be derived by neglecting the core loss of the magnetic ferrite plates as

$$\eta = \frac{i_{2\mathrm{rms}}^2 R_{\mathrm{eq2}}}{i_{1\mathrm{rms}}^2 R_{\mathrm{p1}} + i_{2\mathrm{rms}}^2 \left(R_{\mathrm{eq2}} + R_{\mathrm{p2}}\right)} = \frac{\omega^2 M_{12}^2 R_{\mathrm{eq2}}}{\left[\left(R_{\mathrm{eq2}}+R_{\mathrm{p2}}\right)^2 + \left(\omega L_2 - \frac{1}{\omega C_2}\right)^2\right] R_{\mathrm{p1}} + \omega^2 M_{12}^2 \left(R_{\mathrm{eq2}} + R_{\mathrm{p2}}\right)}. \quad (5)$$

The MEE of the WPT system can be achieved by controlling the duty ratio to satisfy

$$\frac{\partial \eta}{\partial D} = \frac{\partial \eta}{\partial R_{eq2}} \frac{\partial R_{eq2}}{\partial D} = 0 \quad (6)$$

and

$$D_{\mathrm{MEE}} = \frac{1}{\kappa + \frac{\sqrt{2}\pi}{4} \sqrt{\frac{R_{\mathrm{p2}}}{2Lf_{s1} + \kappa\left(R - 2Lf_{s1}\right)}} \sqrt{1 + \frac{\omega^2 M_{12}^2}{R_{\mathrm{p1}} + R_{\mathrm{p2}}}}}. \quad (7)$$

The output power of the system is

$$P_{\mathrm{out}} = \frac{V_{\mathrm{out}}^2}{R} = i_{2\mathrm{rms}}^2 R_{\mathrm{eq2}} = \frac{\omega^2 M_{12}^2 v_{\mathrm{in}}^2 R_{\mathrm{eq2}}}{\left(\omega^2 M_{12}^2 + R_{\mathrm{p1}} R_{\mathrm{p2}} + R_{\mathrm{p1}} R_{\mathrm{eq2}}\right)^2 + \left(R_{\mathrm{p2}} + R_{\mathrm{eq2}}\right)^2 \left(\omega L_1 - \frac{1}{\omega C_1}\right)^2}. \quad (8)$$

The MPP of the WPT system can be achieved by controlling the duty ratio to satisfy

$$\frac{\partial P_{\mathrm{out}}}{\partial D} = \frac{\partial P_{\mathrm{out}}}{\partial R_{eq2}} \frac{\partial R_{eq2}}{\partial D} = 0 \quad (9)$$

and

$$D_{\mathrm{MPT}} = \frac{1}{\kappa + \frac{\sqrt{2}\pi}{4} \sqrt{\frac{R_{\mathrm{p2}}}{2Lf_{s1} + \kappa\left(R - 2Lf_{s1}\right)}} \left(1 + \frac{\omega^2 M_{12}^2}{R_{\mathrm{p1}} + R_{\mathrm{p2}}}\right)}. \quad (10)$$

Apparently, $D_{\mathrm{MPT}} \neq D_{\mathrm{MEE}}$. The control objectives of the WPT system to track the MEE and MPT are different, which confirms the conclusions drawn in [29]. In this paper, the energy efficiency is the primary concern. Therefore, the WPT system is designed to operate under the MEE principle.

III. Minimum Input Power By Phase Angle Control

With any constant output load R, the output voltage V_{out} of the converter is generally regulated at the reference value such that the output power consumed by the load is fixed at the steady state. Therefore, MEE of the WPT system can be achieved by simply minimizing the input current i_s. For this purpose, a hill-climbing-search-based phase angle control is adopted to seek the minimum i_s. Specifically, the phase angle between the arm bridges of the DC/AC converter α is optimized via the phase angle control to regulate v_{in} based on the extended describing function

$$v_{\mathrm{inrms}} = \frac{\sqrt{2}V_{\mathrm{dc}}}{\pi} g\left(\alpha\right), \quad (11)$$

where v_{inrms} is the RMS value of v_{in} and $g(\alpha) = \sqrt{\cos^2\alpha + \sin^2\alpha\cos^2\alpha + 2\cos\alpha + 1}$. Meanwhile, $i_{1\mathrm{rms}}$ (RMS value of i_1) can be derived as

$$i_{1\mathrm{rms}} = \frac{R_{\mathrm{p2}} + R_{\mathrm{eq2}}}{R_{\mathrm{p1}} R_{\mathrm{p2}} + \omega^2 M_{12}^2} v_{\mathrm{inrms}}. \quad (12)$$

According to the energy conservation law and by neglecting the power loss of the DC/AC converter, we have

$$i_s = \frac{v_{\mathrm{inrms}} i_{1\mathrm{rms}}}{V_{\mathrm{dc}}} = \frac{2V_{\mathrm{dc}}^2 \left(R_{\mathrm{P2}} + R_{\mathrm{eq2}}\right)}{\pi^2 \left(R_{\mathrm{P1}} R_{\mathrm{P2}} + \omega^2 M_{12}^2\right)} g^2\left(\alpha\right). \quad (13)$$

Apparently, i_s can be regulated by the phase angle α. Fig. 3 depicts the waveforms of the switching signals and the corresponding waveform of v_{in} (without the resonant tank).

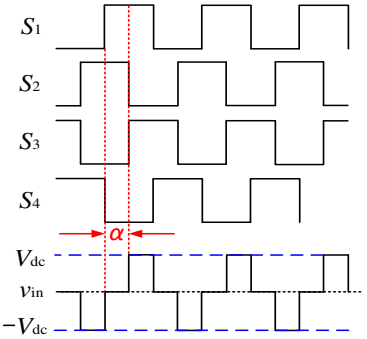

Fig. 3. Waveforms of the switching signals for the DC/AC converter and v_{in} (without the resonant tank).

Fig. 4 depicts the flowchart of the hill-climbing-search-based phase angle control.

The process can be described as follow.

1) An initial phase angle $\alpha(0)$ is applied to the DC/AC converter and the input current $i_s(0)$ is measured.

2) The phase angle α is increased by an incremental angle $\Delta\alpha$ at the next sampling time and the input current $i_s(1)$ is measured.

3) The directions of the hill-climbing search (increase or decrease $\Delta\alpha$) can be determined by the comparison between $i_s(0)$ and $i_s(1)$. If $i_s(1)<i_s(0)$, which means the increase of α approaches the objective of finding the optimal phase angle α_{opt}, α is continuously increased by applying $\alpha(k+1)= \alpha(k)+\Delta\alpha$. Here, k indicates the sampling time kT_s, where T_s is the sampling period of the phase angle control for the DC/AC converter. If $i_s(1)\geqslant i_s(0)$, which means the increase of α deviates from α_{opt}, α is to be decreased by applying $\alpha(k+1)= \alpha(k)-\Delta\alpha$.

4) For both directions of the hill-climbing search, the measured input current at the sampling time $k+1$ are compared to the input current at the previous sampling time k. If $i_s(k+1)<i_s(k)$, which means the tendency of increase or decrease α is correct, $\alpha(k+1)= \alpha(k)+\Delta\alpha$ or $\alpha(k+1)= \alpha(k)-\Delta\alpha$ should continuously be conducted to let α approach α_{opt}. If $i_s(k+1)\geqslant i_s(k)$, which means the change of α cannot further decrease the input current, $\alpha(k)$

can be considered as α_{opt} and the corresponding $i_s(k)$ is the minimum input current.

5) $\alpha(k)$ is used as $\alpha(0)$ for the next iteration to ensure that the minimum input current i_{smin} can always be achieved even if the operating condition of the system is changed. When α_{opt} and i_{smin} are found, the minimum input power of the WPT system can be reached. Meanwhile, if the output voltage of the load is regulated to meet the reference simultaneously, the MEE of the WPT system can be implemented.

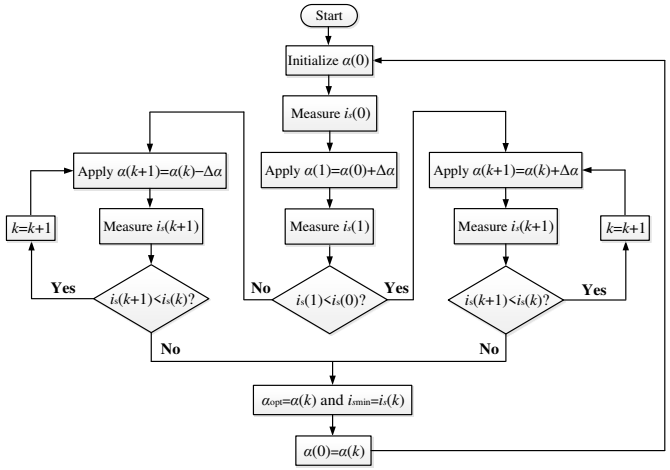

Fig. 4. Flowchart of the hill-climbing-search-based phase angle control.

IV. Output Voltage Regulation by Discrete Sliding Mode Control

Conventionally, the PI control is the common approach for regulating the buck-boost converter of the receiver. Such a controller implemented in the discrete PI control form adopts a control equation

$$\Delta u(k) = K_p \Delta e(k) + K_i e(k), \tag{14}$$

where $\Delta u(k)=u(k)-u(k-1)$ is the increment of the control signal at the sampling time kT_{s1}. T_{s1} is the sampling period of the digital PI control; $e(k)=V_{ref}-V_{out}$ is the error between the reference and the control variable, where V_{ref} is the reference of the output voltage and V_{out} is the measured output voltage; $\Delta e(k)= e(k)-e(k-1)$ is the increment of the error; K_p is the proportional tuning coefficients and K_i is the integral tuning coefficients of the discrete PI controller. Then, the increment of control signal $\Delta u(k)$ is added to the control signal $u(k-1)$ at the previous sampling time to render the present control signal $u(k)$. The control block diagram of the discrete PI control for the WPT system is shown in Fig. 5. Here, β is the coefficient of the output voltage to enable analog-to-digital conversion (ADC) of the digital controller. Specifically, the measured voltage (around 10 V for this case) is out of the range of the ADC requirements (0~3.6V for this case); $V'_{ref}=\beta V_{ref}$ is the scaled down reference; and PWM is short for pulse-width modulation.

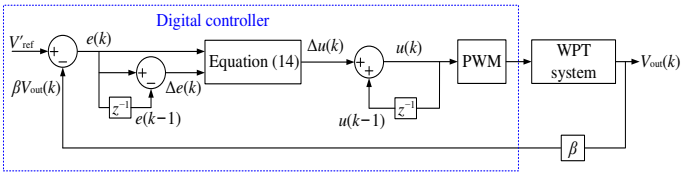

Fig. 5. Control block diagram of the discrete PI control for the WPT system.

However, the use of PI control (since it is a form linear control) limits its effectiveness in giving good voltage regulation to small regions within a predesigned operating point of the WPT system. In the cases of the hill-climbing search process and load-point change, the phase angle will be periodically changed. The output voltage will suffer from high overshoot/undershoot and long settling time during the transient states if the WPT system is regulated by the discrete PI control. To overcome such a dynamic issue, a discrete sliding mode control (DSMC) is therefore adopted to mitigate these undesired phenomena. The control variables $\mathbf{x}(k)$ are expressed in the following form

$$\mathbf{x}(k)=\begin{bmatrix} x_1(k) \\ x_2(k) \\ x_3(k) \end{bmatrix}=\begin{bmatrix} V'_{ref}-\beta V_{out}(k) \\ \dfrac{\beta}{T_{s1}}\left[V_{out}(k)-V_{out}(k+1)\right] \\ T_{s1}\sum_{j=0}^{k-1}\left[V'_{ref}-\beta V_{out}(j)\right] \end{bmatrix}, \tag{15}$$

where β is also defined as the coefficient to enable ADC of the digital controller. Then, the discrete state-space model required for the controller design can be derived as

$$\mathbf{x}(k+1)=\begin{bmatrix} x_1(k+1) \\ x_2(k+1) \\ x_3(k+1) \end{bmatrix}=\begin{bmatrix} 1 & T_{s1} & 0 \\ 0 & 1-\dfrac{T_{s1}}{RC} & 0 \\ T_{s1} & 0 & 1 \end{bmatrix}\begin{bmatrix} x_1(k) \\ x_2(k) \\ x_3(k) \end{bmatrix} + \begin{bmatrix} 0 \\ \dfrac{\beta T_{s1}V_{out}(k)}{LC}-\dfrac{\beta T_{s1}V_{out}(k)}{LC}u(k) \\ 0 \end{bmatrix}. \tag{16}$$

The sliding surface of the DSMC is given as

$$s(k)=\alpha_1 x_1(k)+\alpha_2 x_2(k)+\alpha_3 x_3(k), \tag{17}$$

where α_1, α_2, and α_3 are sliding coefficients. To ensure the stability of the sliding surface, $\alpha_1>0$, $\alpha_2>0$ and $\alpha_3>0$ are preliminary design conditions based on the Routh-Hurwitz criterion. Besides, the local reachability condition of the sliding mode operation must be satisfied [35]

$$\left[s(k+1)-s(k)\right]\mathrm{sgn}\left(s(k)\right)<0, \tag{18}$$

where sgn(.) is the sign function.

If $s(k)\to 0^+$, $s(k+1)<s(k)$. Substitute $u(k)=1$, (16) and (17) into (18) gives

$$0<\left(\frac{\alpha_1\beta L}{\alpha_2}-\frac{\beta L}{RC}\right)i_C(k)-\frac{\alpha_3 LC}{\alpha_2}\left[V'_{ref}-\beta V_{out}(k)\right], \tag{19}$$

where i_C is the output capacitor current.

If $s(k)\to 0^-$, $s(k+1)>s(k)$. Substitute $u(k)=0$, (16) and (17) into (18) gives

$$\left(\frac{\alpha_1\beta L}{\alpha_2}-\frac{\beta L}{RC}\right)i_C(k)-\frac{\alpha_3 LC}{\alpha_2}\left[V'_{ref}-\beta V_{out}(k)\right]<\beta V_{out}(k). \tag{20}$$

Finally, the combination of (19) and (20) gives the simplified existence condition

$$0<\left(\frac{\alpha_1\beta L}{\alpha_2}-\frac{\beta L}{RC}\right)i_C(k)-\frac{\alpha_3 LC}{\alpha_2}\left[V'_{\text{ref}}-\beta V_{\text{out}}(k)\right]<\beta V_{\text{out}}(k). \quad (21)$$

Then, the equivalent control signal $u_{\text{eq}}(k)$ can be obtained by letting $s(k+1)=s(k)$ to give

$$u_{\text{eq}}(k)=1-\frac{K_1}{V'_{\text{ref}}}+\frac{K_1}{\beta V_{\text{out}}(k)}+\frac{K_2 i_C(k)}{\beta V_{\text{out}}(k)}, \quad (22)$$

where $K_1=\frac{\alpha_3 LCV'_{\text{ref}}}{\alpha_2}$ and $K_2=\frac{\beta L}{RC}-\frac{\alpha_1\beta L}{\alpha_2}$ are the tuning coefficients of the DSMC; $0\leqslant u_{\text{eq}}(k)<1$. $u_{\text{eq}}(k)$ can be translated to the instantaneous duty ratio $d(k)$ of the pulse-width modulator [30], which is more suitable for digital controllers. Computational delays (accounting for the time duration of sampling, ADC conversion, PWM reference calculation and updating) and PWM delays (zero-order-hold effect) are approximately 1.5 times sampling periods (T_s and T_{s1}). They are negligible because the sampling frequency of the digital controllers used in this paper is much faster than the switching frequency for the power converters. The control block diagram of the DSMC for the WPT system is shown in Fig. 6.

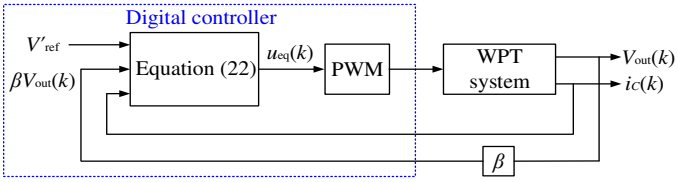

Fig. 6. Control block diagram of the DSMC for the WPT system.

V. Simulation Results

TABLE I. Specifications of Main Components in the WPT System

Parameter	Value	Parameter	Value
V_{dc}	10 V	C_1	27.76 nF
C_2	27.6 nF	R_{p1}	0.441 Ω
R_{p2}	0.415 Ω	L_1	91.24 μH
L_2	91.77 μH	M_{12}	6.3 μH
C_{b}	2 μF	L	50 μH
C	100 μF	R	18 Ω

TABLE II. Parameters of the Controllers

Parameter	Value	Parameter	Value
V_{ref}	10 V	β	0.25
K_{p}	0.4	K_{i}	200
K_1	20	K_2	−0.8
f_s	100 kHz	f_{s1}	20 kHz

Simulation studies are conducted using the software platforms PSIM10 and MATLAB/SIMULINK to compare the performance of the discrete PI control and the DSMC for the WPT system under the MEE principle. The circuit part is implemented in PSIM10 and the control part including the phase angle control, the discrete PI control and the DSMC scheme, are implemented in MATLAB/SIMULINK. A SimCoupler module is used to link up the two software platforms. The sampling frequency for both PSIM10 and MATLAB are set at 14 MHz. The specifications of the main circuit components are listed in Table I. The parameters of the phase angle control, the discrete PI control and the DSMC are provided in Table II. In simulation, β can be implemented as a control block. The switching frequency f_{s1} is the same for both the discrete PI control and the DSMC.

Fig. 7 shows the results of the relationship between the phase angle α, duty ratio of the buck-boost converter d, and the energy efficiency η, when the WPT system is controlled by the phase angle control and the DSMC. As mentioned in [28], the MEE point will only appear at the side of the boundary where the output power decreases with the increase of d. Therefore, only the side with MEE point is investigated. The boundary of the phase angle is 125° and the MEE point is at 110° with a duty ratio of 0.62 and energy efficiency of 69%. The MEE of 69% highly depends on the mutual inductance and the resistance of the load in the WPT system. When the mutual inductance increases (distance between coils reduces), the MEE will increase and vice versa. When the resistance of the load increases, the MEE will decrease and vice versa. Besides, the voltage drops of the diodes in the diode rectifier and the buck-boost converter will distinctly affect the MEE of the WPT system. The steady-state performance of the WPT system controlled by the phase angle control and the DSMC is well verified by matching the results with that of the conventional control scheme.

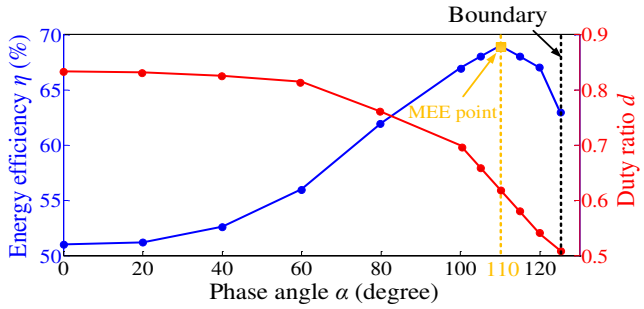

Fig. 7. Relationship between η, d and α when the WPT system is controlled by the phase angle control and the DSMC.

Then, the comparisons of the output voltage V_{out}, the input current i_s, and the instantaneous energy efficiency η between the DSMC and the discrete PI control during transient states are given in Fig. 8−10, respectively. The discrete PI controller is designed for the operating condition of 0° phase angle, such that the parameters of the discrete PI controller are optimally designed for that operating point. Apparently, the dynamic performance of the output voltage V_{out}, the input current i_s, and the instantaneous energy efficiency η are distinctly improved by the DSMC with less overshoot and shorter settling time when the phase angle α is regulated from 40° to 100° with $\Delta\alpha$=20° and the period of 5 ms.

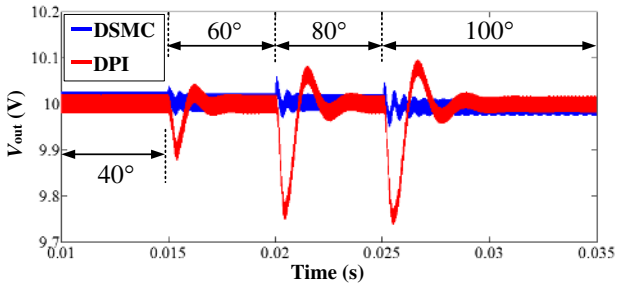

Fig. 8. Comparisons of V_{out} between the discrete PI control and the DSMC for the WPT system.

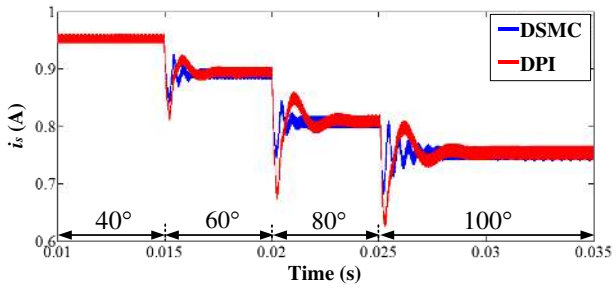

Fig. 9. Comparisons of i_s between the discrete PI control and the DSMC for the WPT system.

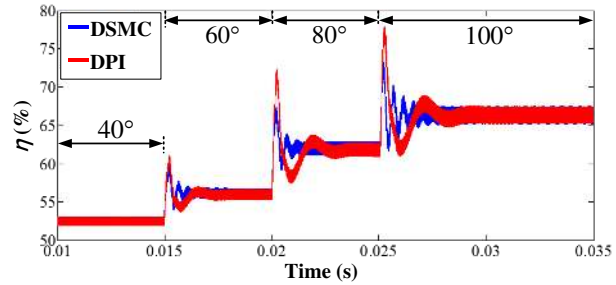

Fig. 10. Comparisons of η between the discrete PI control and the DSMC for the WPT system.

VI. Experimental Verification

The experiment is conducted on a two-coil series-series compensated WPT system with the parameters given in Table I. The parameters of the practical resonators are provided in Table III, where the length of the winding indicates the length from the first turn to the eleventh turn. The controllers used for both the DC/AC converter of the transmitter and the buck-boost converter of the receiver are low-cost MCU STM32VLDISCOVERY with a sampling frequency of 14 MHz. Full schematic diagram of the WPT system in the experiment is depicted in Fig. 11. The codes of the phase angle control based on the algorithm given in Fig. 4 are programmed in the MCU of control stage 1. The codes of the DSMC based on (22) and the discrete PI control based on (14) are programmed in the MCU of control stage 2. A photograph of the experiment setup is shown in Fig. 12.

The experiment is initially carried out with the WPT system controlled by the phase angle control and the DSMC to examine the steady-state performance. Fig. 13 shows the searching process of the input current i_s in reaching the MEE

TABLE III. Parameters of the Practical Resonators

Parameter	Value	Parameter	Value
Coil diameter	31 cm	Wire diameter	1.2 mm
Number of turns	11	Length of the winding	15 mm

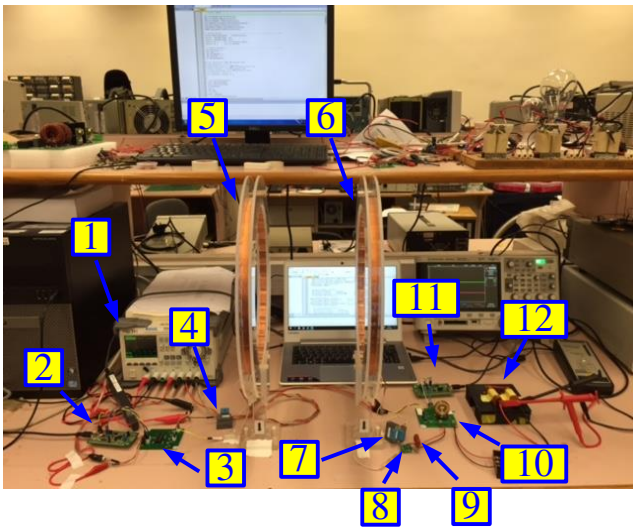

Fig. 12. Photograph of the experiment setup. [1: Power supply for V_{dc} and control stages; 2: STM32DISCOVERY for control stage 1; 3: DC/AC converter; 4: compensated capacitor C_1; 5: Primary winding L_1; 6: Secondary winding L_2; 7: compensated capacitor C_2; 8: diode rectifier; 9: filtering capacitor C_b; 10: Buck-boost converter; 11: STM32DISCOVERY for control stage 2; 12: load R].

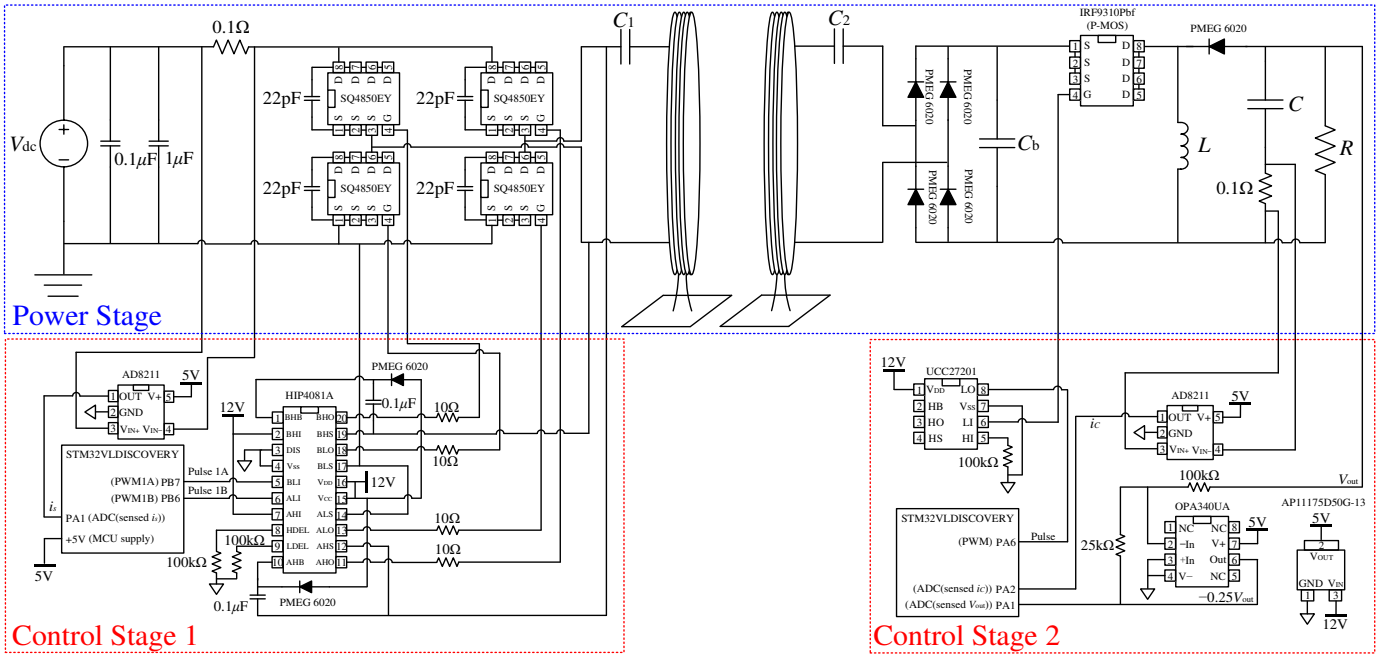

Fig. 11. Full schematic diagram of the WPT system in the experiment.

point of the WPT system. i_s finally reaches the minimum input current at about 0.95A through the regulation of the phase angle control. Besides, the energy efficiency η of the WPT system is calculated and compared. Fig. 14 shows a comparison of the energy efficiency η around the MEE point (the phase angle α, which ranges from 80° to 125° in steps of 5°) between the simulation and the experiment results. As shown, the MEE of the WPT system in practice is about 60%. This is attributed to the diverse energy loss in the hardware (additional voltage drops of diodes, resistance of cables and PCB routes, parasitic resistance of energy storage components, and energy loss in ICs), which are not modelled in the simulation. By applying the conventional control scheme described in [28], the MEE of the WPT system is almost equivalent to 60% as well.

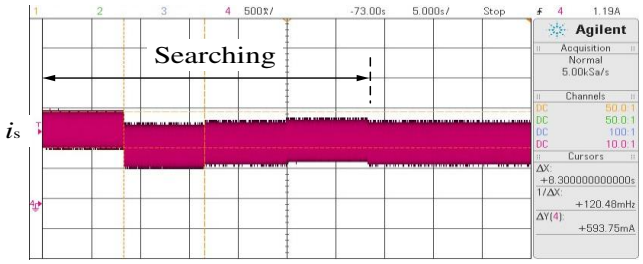

Fig. 13. Search process of the input current i_s to reach the MEE point.

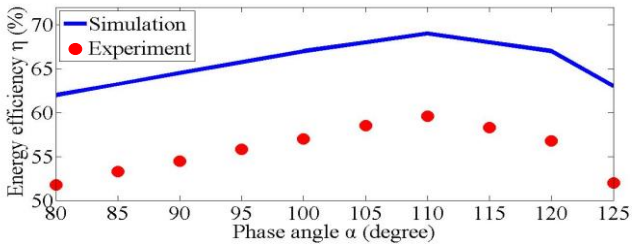

Fig. 14. Comparisons of the energy efficiency η between the simulation and the experiment results.

Then, the comparison of the dynamic performance between the DSMC and the discrete PI control on the MEE tracking process is conducted. The discrete PI controller is designed to operate at 0° phase angle. Fig. 15−18 show the waveforms of the output voltage V_{out} and the corresponding switching signals during both transient and steady states when the buck-boost converter is regulated by the discrete PI control and the DSMC, respectively. In Fig. 15, the overshoot of the output voltage V_{out} during the transient state is about 2.5 V and the settling time is about 151.8 ms when the buck-boost converter is controlled by the discrete PI control when the phase angle α of the DC/AC converter is changed from 120° to 100°. However, as shown in Fig. 16, the overshoot of the output voltage V_{out} during the transient state is about 2 V (80% of that with the discrete PI control) and the settling time is about 48 ms (31.6% of that with the discrete PI control) when the buck-boost converter is controlled by the DSMC with the phase angle α being changed from 120° to 100°.

In Fig. 17, the undershoot of the output voltage V_{out} during the transient state is about 2.0 V and the settling time is about 164.3 ms when the buck-boost converter is controlled by the discrete PI control when the phase angle α is changed from 100° to 110°. However, in Fig. 18, the undershoot of the output voltage V_{out} during the transient state is about 1.9 V and the settling time is about 39.3 ms (23.9% of that with the discrete PI control) when the buck-boost converter is controlled by the DSMC with the phase angle α being changed from 100° to 110°.

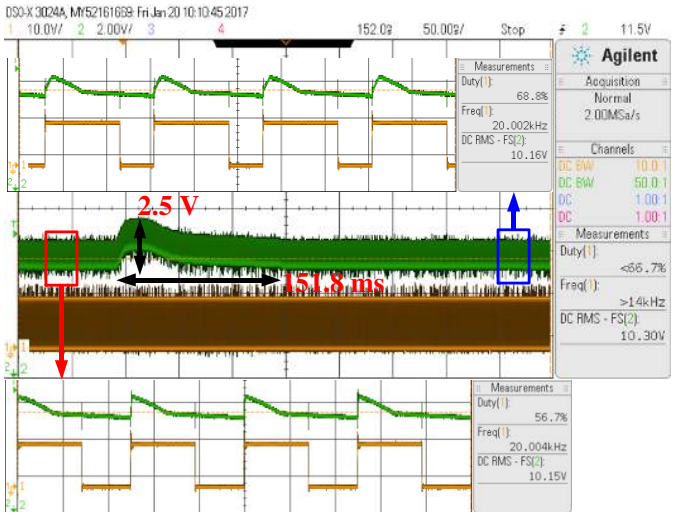

Fig. 15. Waveforms of V_{out} and the corresponding switching signals when the phase angle α is changed from 120° to 100° with the discrete PI control.

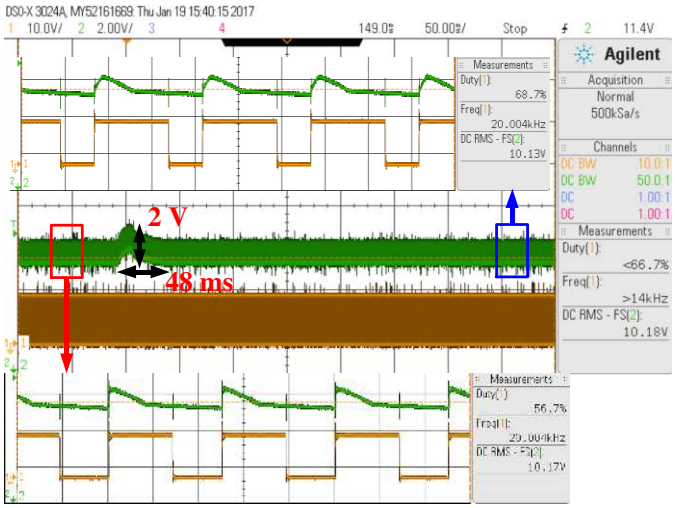

Fig. 16. Waveforms of V_{out} and the corresponding switching signals when the phase angle α is changed from 120° to 100° with the DSMC.

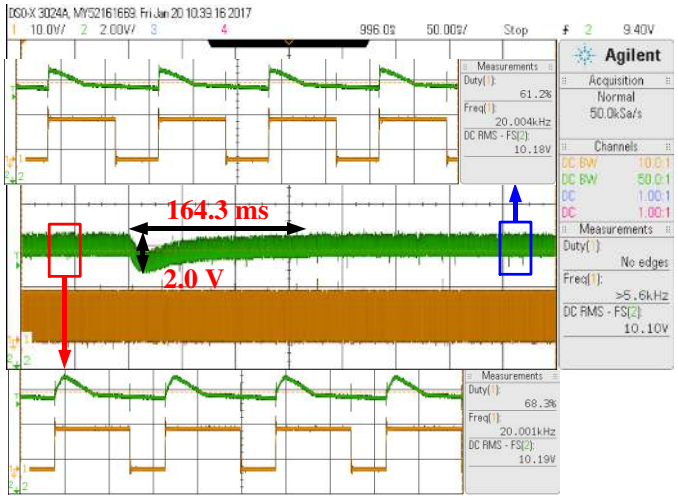

Fig. 17. Waveforms of V_{out} and the corresponding switching signals when the phase angle α is changed from 100° to 110° with the discrete PI control.

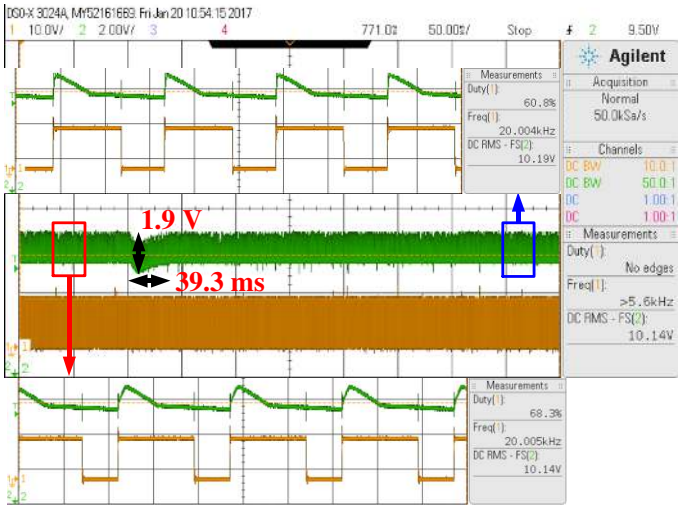

Fig. 18. Waveforms of V_{out} and the corresponding switching signals when the phase angle α is changed from 100° to 110° with the DSMC.

Similar comparisons between the discrete PI control and the DSMC are carried out when the phase angle α varies around the MEE point (80° to 120°) by $\Delta\alpha$=10°. Comparisons of the overshoot/undershoot of the output voltage V_{out} during transient states are illustrated in Fig. 19 using histogram. As shown, the mitigation of the voltage undershoot (with an increasing α) is small with the DSMC scheme. However, the voltage overshoot reduction (with a decreasing α) achievable with the DSMC scheme is significant. The improvement is on average about 16.6%. Comparisons of the settling time of the output voltage V_{out} during transient states are shown in Fig. 20. The settling time is shortened significantly by using the DSMC. The improvement is on average about 72.9%.

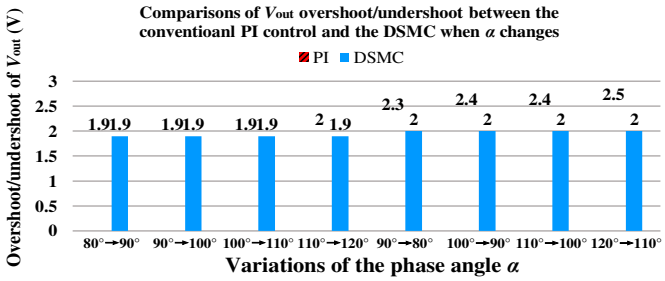

Fig. 19. Comparisons of the overshoot/undershoot of V_{out} between the discrete PI control and the DSMC when α varies around the MEE point.

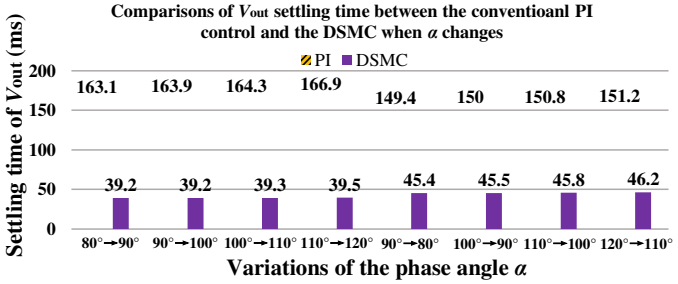

Fig. 20. Comparisons of the setting time of V_{out} between the discrete PI control and the DSMC when α varies around the MEE point.

VII. Conclusions

In this paper, a discrete sliding mode control (DSMC) along with a phase angle control is applied to a two-coil series-series compensated wireless power transfer (WPT) system under the maximum energy efficiency (MEE) principle. Both simulation and experiment results validate that the dynamic performance of the output voltage of the WPT system during the MEE tracking are improved with use of the proposed control scheme, as compared that of the conventional discrete PI control scheme. Experiment results show that the overshoot reduction is about 16.6% and the settling time is shortened by about 72.9% when the phase angle varies around the MEE point in steps of 10°. Such an improvement in the dynamic behavior of the WPT system is important for protecting the load in which it is connected to, from a possible high voltage overshoot during a long transient.

VIII. Acknowledgement

The authors would like to thank Prof. David Hill and the theme-based research project T23-701/14-N.

References

[1] N. Tesla, "Apparatus for transmitting electrical energy," U.S. Patent1119732, Dec. 1, 1914.

[2] W. H. Ko, S. P. Liang, and C. D. F. Fung, "Design of rf-powered coils for implant instruments," *Med. Biol. Eng. Comput.*, vol. 15, pp. 634−640, 1977.

[3] J. G. Bum and B. H. Cho, "An energy transmission system for an artificial heart using leakage inductance compensation of transcutaneous transformer," *IEEE Tran. Power Electron.*, vol. 13, no. 6, pp. 1013−1022, Nov. 1998.

[4] D. Ahn and S. Hong, "Wireless power transmission with self-regulated output voltage for biomedical implant," *IEEE Tran. Ind. Electron.*, vol. 61, no. 5, pp. 2225−2235, May 2014.

[5] W. G. Hurley and J. Kassakian, "Induction heating of circular ferromagnetic plates," *IEEE Tran. Magn.*, vol. 15, no. 4, pp. 1174−1181, Jul. 1979.

[6] G. A. Covic, J. T. Boys, M. L. G. Kissin, and H. G. Lu, "A three-phase inductive power transfer system for roadway-powered vehicles," *IEEE Trans. Ind. Electron.*, vol. 54, no. 6, pp. 3370−3378, Dec. 2007.

[7] J. Huh, S. W. Lee, W. Y. Lee, G. H. Cho, and C. T. Rim, "Narrow-width inductive power transfer system for online electrical vehicles," *IEEE Tran. Power Electron.*, vol. 26, no. 12, pp. 3666−3679, Dec. 2011.

[8] J. Sallán, J. L. Villa, A. Llombart, and J. F. Sanz, "Optimal design of ICPT systems applied to electric vehicle battery charge," *IEEE Tran. Ind. Electron.*, vol. 56, no. 6, pp. 2140−2149, Jun. 2009.

[9] B. Choi, J. Nho, H. Cha, T. Ahn and S. Choi, "Design and implementation of low-profile contactless battery charger using planar printed circuit board windings as energy transfer device," *IEEE Tran. Ind. Electron.*, vol. 51, no. 1, pp. 140−147, Feb. 2004.

[10] Y. Jang and M. M. Jovanovic, "A contactless electrical energy transmission system for portable-telephone battery chargers," *IEEE Tran. Ind. Electron.*, vol. 50, no. 3, pp. 520−527, Jun. 2003.

[11] C.-G. Kim, D.-H.Seo, J.-S. You, J.-H. Park, and B. H. Cho, "Design of a contactless battery charger for cellular phone," *IEEE Tran. Ind. Electron.*, vol. 48, no. 6, pp. 1238−1247, Dec. 2001.

[12] S. Y. R. Hui and W. C. Ho, "A new generation of universal contactless battery charging platform for portable consumer electronic equipment," *IEEE Tran. Power Electron.*, vol. 20, no. 3, pp. 620−627, May 2005.

[13] X. Liu and S. Y. R. Hui, "Simulation study and experimental verification of a contactless battery charging platform with localized charging features," *IEEE Tran. Power Electron.*, vol. 22, no. 6, pp. 2202−2210, Nov. 2007.

[14] S. Y. R. Hui, "Planar inductive battery charging system," U.S. Patent7576514, Aug. 18, 2009.

[15] *Qi System Description: Wireless Power Transfer*, Wireless Power Consortium, Piscataway, NJ, USA, Vol. I: Low Power, Part 1: Interface Definition, Version 1.1, Apr. 2012.

[16] Wireless Power Consortium. (2016). [online]. Available: http://www.wirelesspowerconsortium.com.

[17] M. Budhia, G. A. Covic, J. T. Boys, and C.-Y. Huang, "Development and evaluation of single sided flux couplers for contactless electric vehicle charging," in *IEEE Energy Convers. Congr. Expo. (ECCE)*, Sept. 2011, pp. 614−621.

[18] S. Y. Choi, S. Y. Jeong, E. S. Lee, B. W. Gu, S. W. Lee, and C. T. Rim, "Generalized models on self-decoupled dual pick-up coils for large lateral tolerance," *IEEE Trans. Power Electron.*, vol. 30, no. 11, pp. 6434−6445, Feb. 2015.
[19] J. P. W. Chow, N. Chen, H. S. H. Chung, and L. L. H. Chan, "An investigation into the use of orthogonal winding in loosely coupled link for improving power transfer efficiency under coil misalignment," *IEEE Trans. Power Electron.*, vol. 30, no. 10, pp. 5632−5649, Nov. 2014.
[20] J. Deng, W. Li, T. D. Nguyen, S. Li, and C. C. Mi, "Compact and efficient bipolar coupler for wireless power chargers: design and analysis," *IEEE Trans. Power Electron.*, vol. 30, no. 11, pp. 6130−6140, Mar. 2015.
[21] W. Zhang, S. C. Wong, C. K. Tse, and Q. Chen, "Design for efficiency optimization and voltage controllability of series-series compensated inductive power transfer systems," *IEEE Tran. Power Electron.*, vol. 29, no. 1, pp. 191−200, Jan. 2014.
[22] W. Li, H. Zhao, S. Li, J. Deng, T. Kan, and C. C. Mi, "Integrated LCC Compensation topology for wireless charger in electric and plug-in electric vehicles," *IEEE Tran. Ind. Electron.*, vol. 62, no. 7, pp. 4215−4225, Dec. 2014.
[23] A. K. Swain, M. J. Neath, U. K. Madawala, and D. Thrimawithana, "A dynamic multivariable state-space model for bidirectional inductive power transfer ssytems," *IEEE Tran. Power Electron.*, vol. 27, no. 11, pp. 4772−4780, Nov. 2012.
[24] Z. U. Zahid, Z. M. Dalala, C. Zheng et. al., "Modeling and control of series-series compensated inductive power transfer system," *IEEE J. Emerg. Sel. Topics Power Electron.*, vol. 3, no. 1, pp. 111−123, Mar. 2015.
[25] K. Aditya and S. S. Williamson, "Advanced controller design for a series-series compensated inductive power transfer charging infrastructure using asymmetrical clamped mode control," in *IEEE Applied Power Electron. Confer. Expo. (APEC)*, 2015, pp. 2718−2724.
[26] H. Takanashi, Y. Sato, Y. Kaneko, S. Abe, and T. Yasuda, "A large air gap 3 kW wireless power transfer system for electric vehicles," *IEEE Energy Convers. Cong. Expo. (ECCE)*, 2012, pp. 269−274.
[27] C. K. Lee, W. X. Zhong, and S. Y. R. Hui, "Effects of magnetic coupling of non-adjacent resonators on wireless power domino-resonator systems," *IEEE Tran. Power Electron.*, vol. 27, no. 4, pp. 1905−1916, Apr. 2012.
[28] W. X. Zhong and S. Y. R. Hui, "Maximum energy efficiency tracking for wireless power transfer systems," *IEEE Tran. Power Electron.*, vol. 30, no. 7, pp. 4025−4034, Feb. 2015.
[29] S. Y. R. Hui, W. X. Zhong, and C. K. Lee, "A critical review of recent progress in mid-range wireless power transfer," *IEEE Tran. Power Electron.*, vol. 29, no. 9, pp. 4500−4511, Sept. 2014.
[30] R. Venkataramanan, A. Šabanović, and S. Ćuk, "Sliding mode control of DC-to-DC converters," in *Proceedings of IEEE Conf. Ind. Electron., Control and Instrum.*, 1985, pp. 251−258.
[31] H. Sira-Ramirez and M. Ilic, "A geometric approach to the feedback control of switch mode DC-to-DC power supplies," *IEEE Tran. Circuits Syst.*, vol. 35, no. 10, pp. 1291-1298, Oct. 1988.
[32] S. C. Tan, Y. M. Lai, and C. K. Tse, *Sliding Mode Control of Switching Power Converters – Techniques and Implementation*, Boca Raton: CRC, 2012.
[33] R. J. Wai and L. C. Shih, "Design of voltage tracking control for DC-DC boost converter via total sliding-mode technique," *IEEE Tran. Ind. Electron.*, vol. 58, no. 6, pp. 2502−2511, Aug. 2010.
[34] Y. He and F. Luo, "Sliding-mode control for DC-DC converters with constant switching frequency," *IEE Proceedings Control Theory and Applications*, vol. 153, no. 1, pp. 37−45, Jan. 2006.
[35] S. Z. Sarpturk, Y. Istefanopulos, and O. Kaynak, "On the stability of discrete-time sliding mode control system," *IEEE Trans. Autom. Control*, vol. 32, no. 10, pp. 930−932, Oct. 1987.
[36] W. B. Gao, Y. F. Wang, and A. Homaifa, "Discrete-time variable structure control systems," *IEEE Tran. Ind. Electron.*, vol. 42, no. 2, pp. 117−122, Apr. 1995.
[37] X. Yu and G. Chen, "Discretization behaviors of equivalent control based sliding-mode control systems," *IEEE Trans. Autom. Control*, vol. 48, no. 9, pp. 1641−1646, Sept. 2003.
[38] S.-L. Jung and Y.-Y. Tzou, "Discrete sliding-mode control of a PWM inverter for sinusoidal output waveform synthesis with optimal sliding curve," *IEEE Tran. Power Electron.*, vol. 11, no. 4, pp. 567−577, Jul. 1996.
[39] T.-L. Tai and J.-S. Chen, "UPS inverter design using discrete-time sliding-mode control scheme," *IEEE Tran. Ind. Electron.*, vol. 49, no. 1, pp. 67−75, Aug. 2002.
[40] Y. Yang, W. X. Zhong, S. C. Tan, and S. Y. R. Hui, "Dynamic improvement of wireless power transfer systems with maximum energy efficiency tracking by sliding mode control," in *IEEE Int. Future Energy Electron. Conf. (IFEEC-ECCE Asia)*, Jun. 2017, pp. 1736−1740.

Yun Yang (S'13) received the B.S. degree from Wuhan University, Wuhan, China, in 2012. He is currently working toward the Ph.D. degree in Power Electronics Research Group, Department of Electrical and Electronic Engineering, The University of Hong Kong, Hong Kong. His current research interests include modeling and control of power converters in smart grids, LED lighting systems, and wireless power transfer systems.

Wenxing Zhong (M'13) received his B.Eng. degree in electrical engineering from Tsinghua University, China, in 2007 and Ph.D. degree from the City University of Hong Kong, Hong Kong, in 2012. Currently, he is a professor in the Department of Electrical Engineering, Zhejiang University, China. From Mar. 2016 - May 2017, he was a Research Assistant Professor in the Department of Electrical and Electronic Engineering, The University of Hong Kong, Hong Kong. His current research interests include wireless power transfer and power electronics.

Since 2015, he has received two Transactions First Prize Paper Awards from IEEE Power Electronics Society.

Sitthisak Kiratipongvoot received the B.Eng. and M.Eng. degrees in Electrical Engineering from King Mongkut's University of Technology North Bangkok, Bangkok, Thailand, in 2001 and 2008.

From October 2008 to July 2012, he worked as Research Assistant in Department of Electronic and Information Engineering, Hong Kong Polytechnic University, Hong Kong. Since August 2012, he is a Research Assistant in Department of Electrical and Electronic Engineering, The University of Hong Kong, Hong Kong. His research interests include DC–DC converters, power factor correction AC–DC converters, resonant inverters, soft-switching techniques, renewable energy systems, electric vehicle, and wireless energy transfer.

Siew-Chong Tan received the B.Eng. (Hons.) and M.Eng. degrees in electrical and computer engineering from the National University of Singapore, Singapore, in 2000 and 2002, respectively, and the Ph.D. degree in electronic and information engineering from the Hong Kong Polytechnic University, Hong Kong, in 2005.

From October 2005 to May 2012, he worked as Research Associate, Postdoctoral Fellow, Lecturer, and Assistant Professor in Department of Electronic and Information Engineering, Hong Kong Polytechnic University, Hong Kong. From January to October 2011, he was Senior Scientist in Agency for Science, Technology and Research (A*Star), Singapore. He is currently an Associate Professor in

Department of Electrical and Electronic Engineering, The University of Hong Kong, Hong Kong. Dr. Tan was a Visiting Scholar at Grainger Center for Electric Machinery and Electromechanics, University of Illinois at Urbana-Champaign, Champaign, from September to October 2009, and an Invited Academic Visitor of Huazhong University of Science and Technology, Wuhan, China, in December 2011. His research interests are focused in the areas of power electronics and control, LED lightings, smart grids, and clean energy technologies.

Dr. Tan serves extensively as a reviewer for various IEEE/IET transactions and journals on power, electronics, circuits, and control engineering. He is an Associate Editor of the IEEE Transactions on Power Electronics. He is a coauthor of the book *Sliding Mode Control of Switching Power Converters: Techniques and Implementation* (Boca Raton: CRC, 2011).

Shu Yuen Ron Hui (M'87–SM'94–F'03) received his BSc (Eng) Hons at the University of Birmingham in 1984 and a D.I.C. and PhD at Imperial College London in 1987. Presently, he holds the Philip Wong Wilson Wong Chair Professorship at the University of Hong Kong and a part-time Chair Professorship at Imperial College London. He has published over 300 technical papers, including more than 220 refereed journal publications. Over 60 of his patents have been adopted by industry. He is an Associate Editor of the IEEE Transactions on Power Electronics and IEEE Transactions on Industrial Electronics, and an Editor of the IEEE Journal of Emerging and Selected Topics in Power Electronics. His inventions on wireless charging platform technology underpin key dimensions of Qi, the world's first wireless power standard, with freedom of positioning and localized charging features for wireless charging of consumer electronics. He received the IEEE Rudolf Chope R&D Award from the IEEE Industrial Electronics Society and the IET Achievement Medal (The Crompton Medal) in 2010, and IEEE William E. Newell Power Electronics Award in 2015. He is a Fellow of the Australian Academy of Technological Sciences & Engineering and the Royal Academy of Engineering, U.K.